

Fluoride-Ion-Catalyzed Synthesis of Ladder-type Conjugated Benzobisbenzofurans via Intramolecular Nucleophilic Aromatic Substitution Reaction under Metal-free and Mild Conditions

Katsutoshi Sekino, Naoki Shida, Ryosuke Shiki, Natsuki Takigawa, Hiroki Nishiyama, Ikuyoshi Tomita, and Shinsuke Inagi*

Cite This: <https://dx.doi.org/10.1021/acs.orglett.0c00531>

Read Online

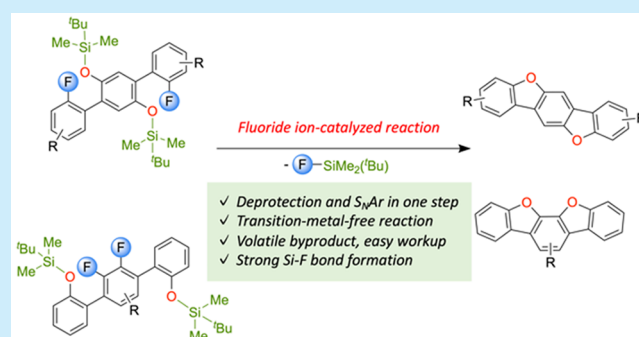
ACCESS |

Metrics & More

Article Recommendations

Supporting Information

ABSTRACT: The fluoride-ion-catalyzed synthesis of benzobisbenzofuran derivatives is described. Fluorine-containing aryl silyl ethers were reacted with 5 mol % of Bu_4NF to give desired compounds in high yield under mild conditions. Syn-selective cyclization reaction was discovered for a particular compound as a kinetic product. Computational analysis revealed that the fluorine substituents in the anti-type benzobisbenzofurans affect the order of the molecular orbitals.



Conjugated ladder polymers are of significant interest for their application in organic electronics due to their outstanding thermal and chemical stability and efficient charge carrier mobility, arising from their planar structure in the main chain.¹ Many conjugated ladder polymers have been synthesized via a postpolymerization cyclization reaction called ladderization.² Heteroatoms are often incorporated into the conjugated backbones due to the expectation for high performances and the synthetic requirements.³ Significant efforts have been devoted to sulfur- and nitrogen-incorporated conjugated ladder polymers, whereas oxygen-incorporated systems, such as ladder-type polybenzofurans (Figure 1), are

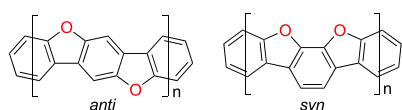


Figure 1. Structures of ladder-type polybenzofurans.

much less studied, presumably due to the lack of ladderization strategy. Still, the oxygen-incorporated conjugated ladder polymers attract a high level of interest based on the studies of the small molecular analogous compounds.⁴

In this Letter, we propose a fluoride-ion-catalyzed nucleophilic aromatic substitution reaction ($\text{S}_{\text{N}}\text{Ar}$) for ladderization, envisioning its future use in the postpolymerization ladderization. Benzobisbenzofurans, which have two dibenzofuran units with one shared benzene ring (i.e., $n = 1$ in Figure 1), are chosen as a model motif because this class of

molecules is the shortest motif of the ladder-type conjugated polybenzofurans.

Several approaches to construct dibenzofuran skeletons have been reported (Figure 2). Intramolecular C–C coupling

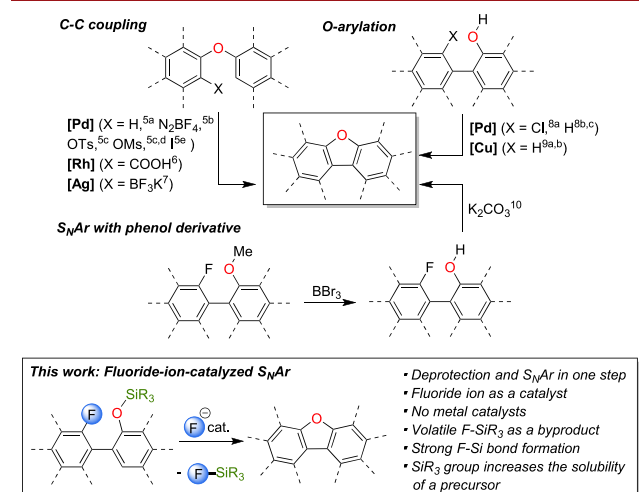
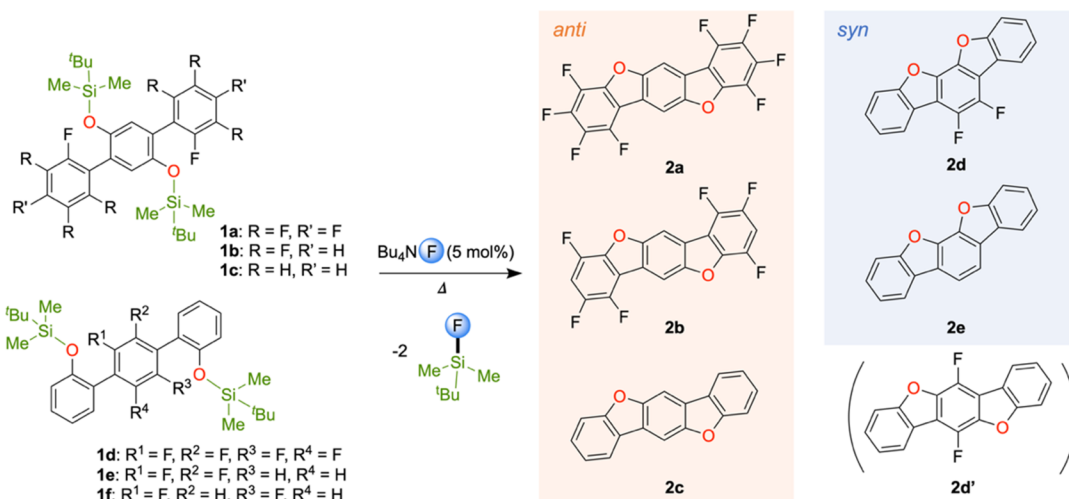


Figure 2. Concept of this work.

Received: February 10, 2020

Table 1. Fluoride-Ion-Catalyzed Formation of Benzobisbenzofuran Derivatives 2a–e



entry ^a	substrate	solvent ^b	temperature (°C)	time (h)	product	yield (%) ^c
1	1a	DMF	80	2	2a	quant.
2	1b	DMF	110	2	2b	96
3	1c	NMP	200	4	2c	80
4	1d	DMF	90	3	2d	quant.
5	1e	DMF	100	3	2e	98
6	1f	NMP	200	5	2c	86

^aSubstrates (**1a**, **1d**–**f**: 95 μmol, **1b**: 64 μmol, **1c**: 19 μmol) were reacted in solvents in the presence of Bu₄NF (5 mol %) under an Ar atmosphere.

^bDMF: *N,N*-dimethylformamide, NMP: *N*-methylpyrrolidone. ^cIsolated yields.

concomitant with C_{sp}²–H activation from diaryl ethers is widely reported with the aid of transition-metal catalysts such as Pd,⁵ Rh,⁶ and Ag.⁷ Another approach is an intramolecular *O*-arylation of 2-arylphenol based on the intramolecular etherification via C–H activation in the presence of Pd⁸ and Cu⁹ catalysts. The third approach is the S_NAr reaction. S_NAr is useful to introduce various functional groups by reacting with nucleophiles without the use of any transition-metal catalysts. Nakano et al. reported the intramolecular S_NAr reaction of 2-(*o*-fluoroaryl)phenol derivatives in the presence of inorganic bases under high-temperature conditions.¹⁰

Our strategy is a one-step approach to construct a dibenzofuran motif from fluorine-containing aryl silyl ethers by using a catalytic amount of external fluoride ions (Figure 2). Such a fluoride-ion-catalyzed S_NAr reaction is recently gaining renewed attention in organic¹¹ and polymer¹² synthesis due to the transition-metal-free nature of the reaction. The reaction proceeds under mild conditions due to the energetic advantage of strong Si–F bond formation. A silyl ether precursor is employed for the reaction instead of phenol derivatives, and thus the solubility of the precursor in common organic solvents is improved, especially in comparison with the corresponding phenol derivatives. Besides that, only volatile trialkylsilyl-fluoride is generated as a byproduct, and thus contamination of the end product by residual metals is avoided. Such impurities can be problematic, especially in the production of the polymeric materials.

The synthetic procedures for precursors **1a**–**c** and **1d**–**f** are described in the Supporting Information. **1a**–**c** were synthesized from 2,5-dibromohydroquinone in five steps (Scheme S1). Because the borylation reaction did not proceed with silyl-protected 2,5-dibromohydroquinone under any conditions attempted, we employed a route to protect 2,5-dibromohydroquinone first with a methoxymethyl (MOM)

group. MOM protection yielded 82% of the product. Subsequently, the bromo group was replaced with boronic acid pinacol ester, followed by deprotection of the MOM group with hydrochloric acid, and then protected again with a *tert*-butyldimethylsilyl (TBS) group, giving a total yield of 22% for three steps. By performing Suzuki–Miyaura coupling with bromopentafluorobenzene, precursors **1a**–**c** were obtained in 63–87% yield. **1d**–**f** were synthesized from 2-hydroxyphenylboronic acid pinacol ester in two steps (Scheme S2). 2-Hydroxyphenylboronic acid pinacol ester was protected by the TBS group to give the products in 90% yield. Then, **1d**–**f** were obtained in 82–94% yield by Suzuki–Miyaura coupling with 1,4-dibromotetrafluorobenzene.

Precursors **1a**–**f** were reacted with 5 mol % Bu₄NF at an elevated temperature under an argon atmosphere. Desired ring-fused compounds **2a**–**e** were obtained in >80% yield (Table 1). The reaction with **1a**, which has five fluorine atoms, completed in 2 h at 80 °C, whereas **1b** bearing four fluorine atoms required 2 h under 110 °C, and **1c** reacted completely in 4 h at 200 °C. This result was attributed to the decreasing electron density of the aromatic ring as the number of fluorines increases, and the phenoxide ion is more likely to attack the aromatic ring. **1d**–**f** reacted to give the cyclized product at 90, 100, and 200 °C, respectively. It is noteworthy that the temperature for the reaction of **1e** is much lower (100 °C for 3 h) than that of 2-(*o*-fluoroaryl)phenol derivative in the presence of K₂CO₃ (165 °C for 18 h), where analogous products are obtained (Figure S1). This result indicates that our strategy can offer mild conditions for the S_NAr-based construction of the benzofuran motif.

Cyclization with **1d** was anticipated to give two isomers, syn-isomer **2d** and anti-isomer **2d'**. However, the reaction with **1d** completed in 3 h under 90 °C to give one isomer exclusively. The ¹³C{H} NMR spectrum of the isolated product showed a

double doublet peak at 141 ppm with coupling constants of 247.5 and 15.8 Hz, indicating one-bond and two-bond couplings with fluorine atoms, respectively.¹³ These data strongly suggest the formation of syn-isomer **2d**. Single-crystal X-ray structure analysis was also performed for the product to confirm the formation of **2d** (Figure S2). **2d** showed a planar structure with a herringbone packing. The minimum face-to-face distance was 3.35 Å, whereas that of nonfluorinated analogue **2e** was 3.49 Å (Figure S3).¹⁴ This result suggests a stronger π - π interaction in **2d** than **2e**, presumably due to the intermolecular interaction of the donor unit and the acceptor unit in the crystalline structure of **2d**.¹⁵ Multiple hydrogen bonds between F-H and O-H were also confirmed in the crystal structure of **2d**. These interactions are also reflected in the melting point of this molecule. The melting point of **2d** was 280 °C, whereas the melting point of **2e** was 185 °C. All of these results suggest the significant effect of the introduction of fluorine atoms in the conjugated backbone.

The reaction conditions required for **1e** and **1f** were surprisingly different, although the number of fluorine atoms in the central aromatic rings was equally two. The reaction with **1e**, where two fluorine atoms locate at the ortho position, smoothly proceeded at 100 °C to give syn-product **2e**. On the contrary, the reaction of **1f**, where two fluorine atoms locate at the para position to give anti-product **2c**, required 200 °C for the completion. The difference in the reaction conditions observed here seems to stem from the comparable reason for the exclusive production of syn-product **2d** from **1d**.

To gain more insight into the selectivity of the reaction of **1d**, computational simulations were performed with density functional theory (DFT). Calculations were performed at the B3LYP or ω B97XD level of theory. Optimizations and single-point calculations were performed on **2d** and **2d'** as well as the one-sided fused products of **1d**. The corresponding Meisenheimer intermediates and transition states were also successfully simulated. The rate-determining step in common S_NAr reactions is the nucleophilic attack, whereas the elimination step is much faster.¹⁶ Therefore, the transition states for the elimination step are not discussed. The energy diagrams of these products are shown in Figures S4–S6. There was only a slight difference in the energies of the end products **2d** and **2d'** (<0.20 kcal/mol). The charge density of the carbon atom connected to the fluorine atom in the one-sided cyclized product was found to be affected by the geometry, although the charge differences between C_{para} and C_{ortho} were quite small in any case (Figures S4 and S5). Thus the exclusive production of syn-type **2d** is not attributed to these factors. The transition state to give syn-type was 1.1 to 1.5 kcal/mol more stable than that of anti-type (Figures S6 and S7). This trend was also confirmed when a single-point calculation was performed with the B3LYP-D3 level of theory using the 6-311G+(2df,2p) basis set including the solvent effect (Figure S8). From these calculations, it was concluded that **2d** was obtained as a kinetic product. This result also explains the reason for the milder reaction condition required for **1e** than that for **1f**, where the kinetic barrier for **1e** was probably smaller than that for **1f**. The cyclization of **1d** at a high temperature (200 °C) in NMP solely afforded **2d** due to the irreversibility of the reaction (Scheme S3).

The plausible mechanism of this reaction is shown in Figure 3. First, the fluoride ion derived from Bu_4NF deprotects the silyl ether to generate a phenoxide ion. The phenoxide ion causes an intramolecular nucleophilic attack on the fluorinated

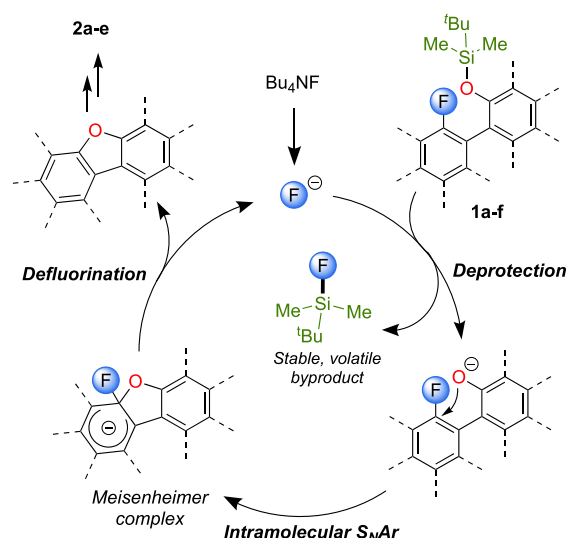


Figure 3. Plausible reaction mechanism.

aromatic ring to form a Meisenheimer complex, followed by the elimination of the fluoride ion. Because the fluoride ion is regenerated upon the reaction, this reaction proceeds with a catalytic amount of fluoride ions (Figure 3).

UV-vis absorption and fluorescence (FL) measurements and cyclic voltammetry (CV) measurements were performed for product **2a–e**. The absorption and FL spectra showed mirror images, suggesting the structural rigidity of these molecules (Figure 4 and Table S2). The largest absorption peaks of **2a–c** appeared at 312, 311, and 329 nm, respectively, indicating that the introduction of fluorine atoms causes the blue shift of λ_{max} in anti-type molecules. Absorption spectra of

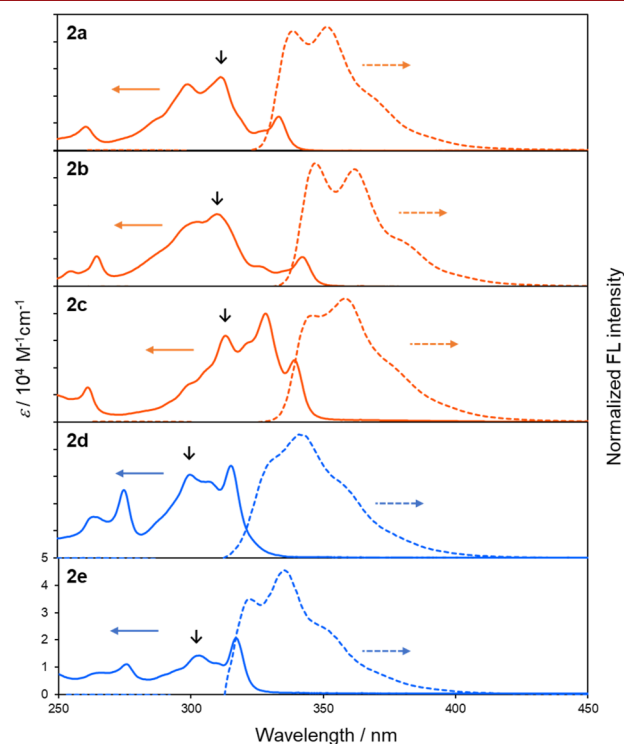


Figure 4. Absorption (solid line) and FL (dashed line) spectra of **2a–e**. Black arrows indicate the excitation wavelength for the FL measurement.

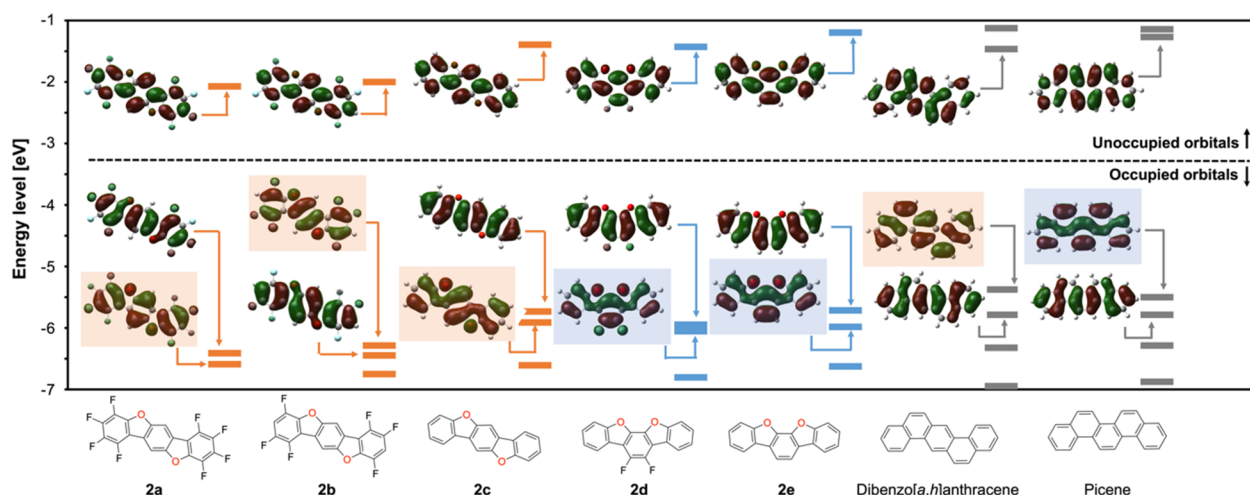


Figure 5. Orbital energy levels around the frontier orbital of **2a–e**, dibenzo[*a,h*]anthracene, and picene simulated at the B3LYP/6-31G(d) level theory. MOs of the HOMO–1, HOMO, and LUMO are described (iso value = 0.02).

2a–c showed characteristic peaks in the 340–350 nm region. Similar transitions have also been reported for the anti-type benzobisbenzothiophenes.¹⁷ For syn-type molecules, λ_{max} of **2d,e** was 316 and 317 nm, respectively. Because the Stokes shifts for **2c–e** were small, FL spectra were collected under the excitation at 314, 300, and 303 nm for **2c–e**, respectively, instead of exciting with the wavelength of the largest absorption. The normalized FL spectra were identical under different excitation wavelengths (Figure S9). Anti-type compounds **2a–c** showed higher internal quantum efficiency ($\phi_{\text{F}} = 0.57$ to 0.64) compared with syn-type **2d,e** ($\phi_{\text{F}} = 0.25$ to 0.44) (Table S2). This is probably because the anti-type molecules show less self-absorption than syn molecules. The electrochemical properties were evaluated by CV measurement (Figure S12). All compounds **2a–e** showed irreversible redox behavior in 0.1 M Bu₄NPF₆/CH₂Cl₂.

To better understand the electronic structure of **2a–e**, molecular orbitals (MOs) of these compounds were simulated with DFT calculation at the B3LYP/6-31G(d) level of theory. Isoelectronic compounds, dibenzo[*a,h*]anthracene and picene, were also simulated for comparison. Previously, it was reported that the HOMOs of benzo[2,1-*b*:3,4-*b'*]dithiophene derivatives corresponded to that of picene, whereas its oxygen analogue showed a different shape in the HOMO, suggesting that the elements incorporated at the bridging position significantly affect its MOs.¹⁸ Among the compounds prepared in this study, we found that the HOMO of anti-product **2a,c** or syn-product **2d,e** resembled the HOMO–1 of dibenzo[*a,h*]anthracene or picene, respectively. Accordingly, the HOMO–1 of **2a,c** and **2d,e** corresponds to the HOMOs of dibenzo[*a,h*]anthracene and picene, respectively (Figure 5, highlighted). On the contrary, **2b** showed exceptional order in MOs. The HOMO of **2b** corresponds to those of dibenzo[*a,h*]anthracene, whereas the HOMO–1 showed the shape of the HOMO–1 of dibenzo[*a,h*]anthracene. This result suggests that the substituents in the aromatic ring can alter the MOs in this type of molecule. This tendency was also confirmed when the simulation was performed with the B3LYP-D3/def2TZVP level of theory (Figure S13).

TD-DFT analysis was performed for anti-type molecules **2a–c** at the B3LYP/6-311G+(2df,2p) level of theory. **2a–c** showed two transitions in the 300–350 nm region (Figures S14–16, Table S4). Although the simulated transitions were

blue-shifted compared with the experimental data, TD-DFT well simulated each transition observed in the experimental spectra. The TD-DFT simulation revealed that transitions at the lowest energy region arise from the significant contribution of highlighted occupied orbitals (see Figure 5) to the LUMO (Table S4).

In conclusion, we have successfully synthesized various benzobisbenzofuran derivatives by using an intramolecular S_NAr reaction with fluoride ions as a catalyst under mild conditions. This system has features such as a high yield, no use of a transition-metal catalyst, and high solubility of the precursor derived from the silyl group, which are ideal for the postpolymerization ladderization to address the variety of ladder-type conjugated polymers.

■ ASSOCIATED CONTENT

Supporting Information

The Supporting Information is available free of charge at <https://pubs.acs.org/doi/10.1021/acs.orglett.0c00531>.

General experimental procedure, material information, reaction conditions, and spectroscopic data (PDF)

Accession Codes

CCDC 1974979 contains the supplementary crystallographic data for this paper. These data can be obtained free of charge via www.ccdc.cam.ac.uk/data_request/cif, or by emailing data_request@ccdc.cam.ac.uk, or by contacting The Cambridge Crystallographic Data Centre, 12 Union Road, Cambridge CB2 1EZ, UK; fax: +44 1223 336033.

■ AUTHOR INFORMATION

Corresponding Author

Shinsuke Inagi – Department of Chemical Science and Engineering, School of Materials and Chemical Technology, Tokyo Institute of Technology, Yokohama 226-8502, Japan; PRESTO, Japan Science and Technology Agency (JST), Saitama 332-0012, Japan; orcid.org/0000-0002-9867-1210; Email: inagi@cap.mac.titech.ac.jp

Authors

Katsutoshi Sekino – Department of Chemical Science and Engineering, School of Materials and Chemical Technology, Tokyo Institute of Technology, Yokohama 226-8502, Japan

Naoki Shida – Department of Chemical Science and Engineering, School of Materials and Chemical Technology, Tokyo Institute of Technology, Yokohama 226-8502, Japan

Ryosuke Shiki – Department of Chemical Science and Engineering, School of Materials and Chemical Technology, Tokyo Institute of Technology, Yokohama 226-8502, Japan

Natsuki Takigawa – Department of Chemical Science and Engineering, School of Materials and Chemical Technology, Tokyo Institute of Technology, Yokohama 226-8502, Japan

Hiroki Nishiyama – Department of Chemical Science and Engineering, School of Materials and Chemical Technology, Tokyo Institute of Technology, Yokohama 226-8502, Japan

Ikuyoshi Tomita – Department of Chemical Science and Engineering, School of Materials and Chemical Technology, Tokyo Institute of Technology, Yokohama 226-8502, Japan;

orcid.org/0000-0003-3995-5528

Complete contact information is available at:

<https://pubs.acs.org/10.1021/acs.orglett.0c00531>

Notes

The authors declare no competing financial interest.

ACKNOWLEDGMENTS

This study was supported by a Support for Tokyo Tech Advanced Researchers (STAR) grant funded by the Tokyo Institute of Technology Fund (Tokyo Tech Fund). We thank Dr. Yoshihisa Sei at the Suzukakedai Materials Analysis Division, Technical Department, Tokyo Institute of Technology for single-crystal X-ray analysis.

REFERENCES

- (1) (a) Lee, J.; Kalin, A. J.; Yuan, T.; Al-Hashimi, M.; Fang, L. Fully Conjugated Ladder Polymers. *Chem. Sci.* **2017**, *8*, 2503–2521. (b) Zhu, C.; Kalin, A. J.; Fang, L. Covalent and Noncovalent Approaches to Rigid Coplanar π -Conjugated Molecules and Macromolecules. *Acc. Chem. Res.* **2019**, *52*, 1089–1100.
- (2) (a) Takagi, K.; Kato, R.; Yamamoto, S.; Masu, H. Amide-bridged ladder poly(*p*-phenylene): synthesis by direct arylation and π -stacked assembly. *Polym. Chem.* **2015**, *6*, 6792–6795. (b) Daigle, M.; Morin, J.-F. Helical Conjugated Ladder Polymers: Tuning the Conformation and Properties through Edge Design. *Macromolecules* **2017**, *50*, 9257–9264. (c) Hollingsworth, W. R.; Lee, J.; Fang, L.; Ayzner, A. L. Exciton Relaxation in Highly Rigid Conjugated Polymers: Correlating Radiative Dynamics with Structural Heterogeneity and Wavefunction Delocalization. *ACS Energy Lett.* **2017**, *2*, 2096–2102. (d) Yin, Y.; Zhang, S.; Chen, D.; Guo, F.; Yu, G.; Zhao, L.; Zhang, Y. Synthesis of an Indacenodithiophene-based Fully Conjugated Ladder Polymer and its Optical and Electronic Properties. *Polym. Chem.* **2018**, *9*, 2227–2231. (e) Trilling, F.; Auslander, M.-K.; Scherf, U. Ladder-Type Polymers and Ladder-Type Polyelectrolytes with On-chain Dibenz[*a,h*]anthracene Chromophores. *Macromolecules* **2019**, *52*, 3115–3122.
- (3) (a) Mei, J.; Diao, Y.; Appleton, A. L.; Fang, L.; Bao, Z. Integrated Materials Design of Organic Semiconductors for Field-Effect Transistors. *J. Am. Chem. Soc.* **2013**, *135*, 6724–6746. (b) Anthony, J. E. Functionalized Acenes and Heteroacenes for Organic Electronics. *Chem. Rev.* **2006**, *106*, 5028–5048.
- (4) Tsuji, H.; Nakamura, E. Design and Functions of Semi-conducting Fused Polycyclic Furans for Optoelectronic Applications. *Acc. Chem. Res.* **2017**, *50*, 396–406.
- (5) (a) Liégault, B.; Lee, D.; Huestis, M. P.; Stuart, D. R.; Fagnou, K. Intramolecular Pd(II)-Catalyzed Oxidative Biaryl Synthesis under Air: Reaction Development and Scope. *J. Org. Chem.* **2008**, *73*, 5022–5028. (b) Du, Z.; Zhou, J.; Si, C.; Ma, W. Synthesis of Dibenzofurans by Palladium-Catalyzed Tandem Denitration/C-H Activation. *Synlett* **2011**, *2011*, 3023–3025. (c) Nervig, C. S.; Waller, P. J.; Kalyani, D. Palladium-Catalyzed Intramolecular C-H Arylation of Arenes Using Tosylates and Mesylates as Electrophiles. *Org. Lett.* **2012**, *14*, 4838–4841. (d) Ferguson, D. M.; Rudolph, S. R.; Kalyani, D. Palladium-Catalyzed Intra- and Intermolecular C-H Arylation Using Mesylates: Synthetic Scope and Mechanistic Studies. *ACS Catal.* **2014**, *4*, 2395–2401. (e) Panda, N.; Mattan, I.; Nayak, D. K. Synthesis of Dibenzofurans via C-H Activation of *o*-Iodo Diaryl Ethers. *J. Org. Chem.* **2015**, *80*, 6590–6597.
- (6) Maetani, S.; Fukuyama, T.; Ryu, I. Rhodium-Catalyzed Decarbonylative C-H Arylation of 2-Aryloxybenzoic Acids Leading to Dibenzofuran-derivatives. *Org. Lett.* **2013**, *15*, 2754–2757.
- (7) Lockner, J. W.; Dixon, D. D.; Risgaard, R.; Baran, P. S. Practical Radical Cyclizations with Arylboronic Acids and Trifluoroborates. *Org. Lett.* **2011**, *13*, 5628–5631.
- (8) (a) Kawaguchi, K.; Nakano, K.; Nozaki, K. Synthesis of Ladder-Type π -Conjugated Heteroacenes via Palladium-Catalyzed Double N-Arylation and Intramolecular O-Arylation. *J. Org. Chem.* **2007**, *72*, 5119–5128. (b) Wei, Y.; Yoshikai, N. Oxidative Cyclization of 2-Arylphenols to Dibenzofurans under Pd(II)/Peroxybenzoate Catalysis. *Org. Lett.* **2011**, *13*, 5504–5507. (c) Xiao, B.; Gong, T. J.; Liu, Z. J.; Liu, J. H.; Luo, D. F.; Xu, J.; Liu, L. Synthesis of Dibenzofurans via Palladium-Catalyzed Phenol-Directed C-H Activation/C-O Cyclization. *J. Am. Chem. Soc.* **2011**, *133*, 9250–9253.
- (9) (a) Zhao, J.; Wang, Y.; He, Y.; Liu, L.; Zhu, Q. Cu-Catalyzed Oxidative C(sp²)-H Cycloetherification of *o*-Arylphenols for the Preparation of Dibenzofurans. *Org. Lett.* **2012**, *14*, 1078–1081. (b) Liu, J.; Fitzgerald, A. E.; Mani, N. S. Facile Assembly of Fused Benzo[4,5]Furo Heterocycles. *J. Org. Chem.* **2008**, *73*, 2951–2954.
- (10) Truong, M. A.; Nakano, K. Syntheses of Dibenzofuro[2,1-*b*:3,4-*b'*]Difuran-derivatives and Their Application to Organic Field-Effect Transistors. *Beilstein J. Org. Chem.* **2016**, *12*, 805–812.
- (11) Liu, C.; Zang, X.; Yu, B.; Yu, X.; Xu, Q. Microwave-Promoted TBAF-Catalyzed S_NAr Reaction of Aryl Fluorides and ArSTMS: An Efficient Synthesis of Unsymmetrical Diaryl Thioethers. *Synlett* **2011**, 1143–1148.
- (12) (a) Wang, Y.; Watson, M. D. Transition-metal-free Synthesis of Alternating Thiophene-Perfluoroarene Copolymers. *J. Am. Chem. Soc.* **2006**, *128*, 2536–2537. (b) Dutta, T.; Woody, K. B.; Watson, M. D. Transition-metal-free Synthesis of Poly(phenylene Ethynylene)s with Alternating Aryl-Perfluoroaryl Units. *J. Am. Chem. Soc.* **2008**, *130*, 452–453. (c) Sanji, T.; Iyoda, T. Transition-metal-free Controlled Polymerization of 2-Perfluoroaryl-5-trimethylsilylthiophenes. *J. Am. Chem. Soc.* **2014**, *136*, 10238–10241.
- (13) Chertkov, V. A.; Sergeyev, N. M. Proton-Coupled ¹³C NMR Spectra of Fluorobenzene. *J. Magn. Reson.* **1976**, *21*, 159–163.
- (14) Karlsson, B.; Pilotti, A.-M.; Söderholm, A.-C. Quinone Oligomerization. V. Structure of Benzo[1,2-*b*:6,5-*b'*]Bis[1]Benzofuran, C₁₈H₁₀O₂. *Acta Crystallogr., Sect. C: Cryst. Struct. Commun.* **1983**, *39*, 1275–1277.
- (15) Thalladi, V. R.; Weiss, H.-C.; Bläser, D.; Boese, R.; Nangia, A.; Desiraju, G. R. C-H...F Interactions in the Crystal Structures of Some Fluorobenzenes. *J. Am. Chem. Soc.* **1998**, *120*, 8702–8710.
- (16) Senger, N. A.; Bo, B.; Cheng, Q.; Keeffe, J. R.; Gronert, S.; Wu, W. The Element Effect Revisited: Factors Determining Leaving Group Ability in Activated Nucleophilic Aromatic Substitution Reactions. *J. Org. Chem.* **2012**, *77*, 9535–9540.
- (17) Wang, Y.; Parkin, S. R.; Gierschner, J.; Watson, M. D. Highly Fluorinated Benzobisbenzothiophenes. *Org. Lett.* **2008**, *10*, 3307–3310.
- (18) Truong, M. A.; Nakano, K. Syntheses and Properties of Ladder-Type π -Conjugated Compounds Containing a Benzo[2,1-*b*:3,4-*b'*]Dithiophene Skeleton. *Bull. Chem. Soc. Jpn.* **2016**, *89*, 1034–1040.